PROCEEDINGS OF THE INTERNATIONAL CONFERENCE NANOMATERIALS: APPLICATIONS AND PROPERTIES
Vol. 4 No 2, 02CBNM01(4pp) (2015)

Study on Microstructure and Ablation Properties of Graphene Oxide/Zirconium Diboride Nanoparticle/Carbon Fiber/Resol Nanocomposites

Z. Amirsardari, M. Salavati-Niasari*

Institute of Nano Science and Nano Technology, University of Kashan, Kashan, P.O. Box 87317-51167, I. R. Iran

(Received 27 March 2015; published online 22 August 2015)

The development of compatible additives for hot corrosion inhibition in high temperature application requires test methods which yield significant results on a short time scale. The present study aims at the evaluation of the effect of hot corrosion inhibiting model additives on the performance of an ablative phenolic resin using oxy-acetylene torch test which measure different properties. Thermogravimetric analysis (TGA) and field-emission scanning electron microscopy (FESEM) in combination with energy disperse X-ray (EDX) are used. Two kinds of corrosion inhibiting additives are employed: an inorganic inhibitor based on graphene oxide sheets (GO); a ceramic nanoparticle (ZrB_2) with inhibiting properties. The results obtained show that hot corrosion inhibiting additives drastically modify the ablation and thermal stability. The experimental approach described in this paper should be useful for additive development in carbon fiber/phenolic composite because it yields a more durable product than can be obtained by neat composite of how a given additive affects the ablation performance in a hot corrosive environment.

Keywords: Carbon Fiber/phenolic composite, Ceramic nanoparticles, Hot corrosion inhibition, Thermal stability.

PACS number(s): 72.80.Tm, 62.23.Pq, 68.60.Dv

1. INTRODUCTION

For thermal protection systems two very different classes of materials have been considered: carbon fiber composites, and ultra-high temperature ceramics [1]. The charring ablators are the most widely used thermal protection shields, and based on the facts that an improvement in flammability properties of polymers has been obtained with graphene nanofillers that provided another candidate as a synergist agent due to its unique two-dimensional (2D) atomic carbon sheet structure [2]. The graphene sheets act as effective cross-link junctions and can produce network structure in the char layer and improve the char layer resistance against stripping during high flow rate of hot gases [3]. Also, the oxidation onset temperature of organic resins can be increased by the ceramic particles such as zirconium diboride (ZrB_2) [4]. ZrB_2–based ceramics are included in the so-called ultra-high-temperature ceramics (UHTC) with potential applications in the industry because of its electrical and thermal conductivities, good oxidation and chemical attack resistances [5].

In the oxidative conditions, researchers reported the formation of an oxide scale containing boria (B_2O_3) and zirconia (ZrO_2) layers upon the surface which directly cuts the diffusion channel for oxygen [6]. ZrO_2 has a thermal barrier property which forms a layer to protect the degradation of underlying nanocomposite. An increase in temperature gradient noticeably differentiates the sample at high heating times because of the difficult dissipation of heat from the surface, which accelerated high temperature oxidation and fracture [7]. The magnitude of the temperature gradient decreases with the two additives in composites to observe synergetic effects, improve in thermal conductivity and prevent the diffusion of oxygen. Different thermal radiation and conduction abilities of ZrB_2 and GO dominate various surface temperatures.

Using GO and ZrB_2 as reinforcements to control hot corrosion of carbon/phenolic composite at 2000°C is enhanced thermal resistance of phenolic composites due to ZrO_2 and char layer in reduction of ablation rate.

2. EXPERIMENTAL SECTION

Zirconium n-propoxide ($Zr(OPr)_4$, Sigma-Aldrich) and Phenolic resin (PR, Resitan Co.) based on a phenolic resol type resin were used in the present process. All of reagents and solvents were obtained from Merck. The salen ligand and GO were prepared according to previous work [8, 9]. To a solution of the zirconium (IV) n-propoxide, H_2salen, methanol and dionized water was added boric acid in acetic acid followed by citric acid at room temperature. The resulting mixture was dried at 120°C. Afterward, it was placed into a tubular furnace at 1500°C for 2h under argon atmosphere. Finally, ZrB_2 nanopowder was obtained.

The Zr/GO/PR composites were prepared by dispersing 1 wt% of GO and 7 wt% of ZrB_2 nanoparticles in the resol solution, and then dispersed by ultrasound for 1 h at room temperature. The solution was added into carbon fibers (CF). The mixture was dried at 70°C. The composites were cured at 150°C for 2 h in hot press. Two types composites were fabricated by this procedure: carbon- phenolic resin (PR), and ZrB_2/GO/carbon-phenolic (Zr/GO/PR).

Field emission scanning electron microscopy (FESEM, Mira 2 Tescan) was applied to study the microstructure of the samples. The thermal stability of the produced materials was investigated using a TGA instrument (Linseys STA 1600). Measurements conducted in nitrogen at dynamic scans of 10°C/min from

* salavati@kashanu.ac.ir

 © 2015 Sumy State University

30°C to 1000°C. The ablation performance was operated at an oxyacetylene test bed. The gun was set at a stand-off distance of 5 cm relative to the samples. The samples were cut into a size of 2.5 cm in diameter and 2 cm in height for ablation test, and held in position using a stainless fixture and exposed for 160 s.

3. RESULTS AND DISCUSSION

3.1 The XRD analysis of ZrB_2 nanoparticles

The XRD pattern of ZrB_2 nanoparticles is shown in Fig. 1a. The pattern of ZrB_2 was indexed as a pure hexagonal structure. In order to explore the ZrB_2 nanoparticle size and morphological characteristics in more detail, FESEM (Fig. 1b) analysis was performed. The image showed small spherical and uniform nanoparticles with the size of about 30 nm in diameter.

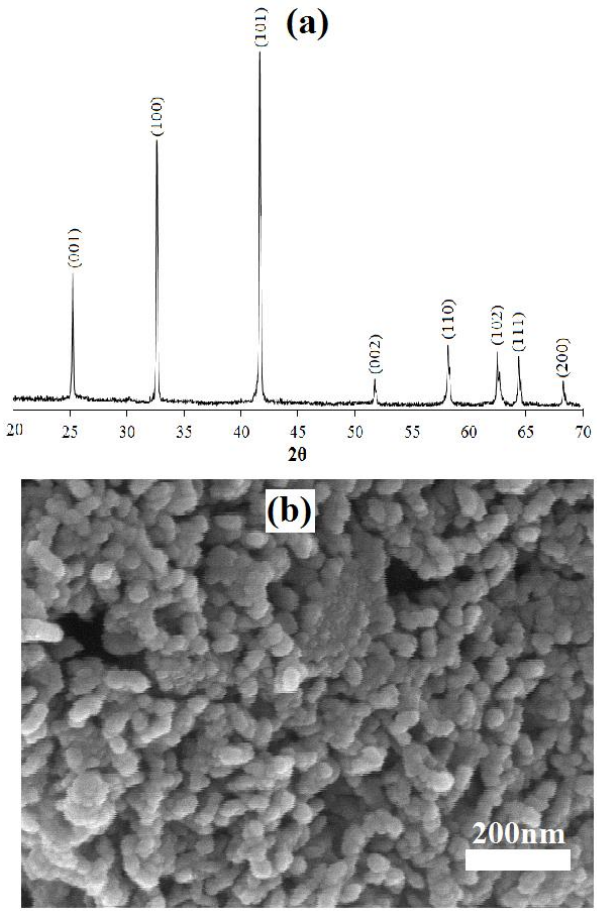

Fig. 1 – (a) XRD pattern and (b) FESEM image of ZrB_2 nanoparticles pyrolyzed at 1500°C

3.2 Thermogravimetric analysis

Figure 2 presents the TGA and derivative TGA (DTGA) curves of PR, and Zr/GO/PR composites under nitrogen atmosphere. The maximum temperature of decomposition of the phenolic composite occurred at about 460°C, and maximum weight loss percent was 23%. The addition of nanoparticles led to a reduction in the residual mass of PR at 1000°C [10]. Graphene oxide exfoliates and decomposes when rapidly heated to ~1050°C which exhibits a distinct weight loss [11, 12]. Incorporating these particles could further enhance the thermal stability of PR due to the incomplete oxidation of the charred material and composition of ZrO_2 at higher temperature than 1000°C.

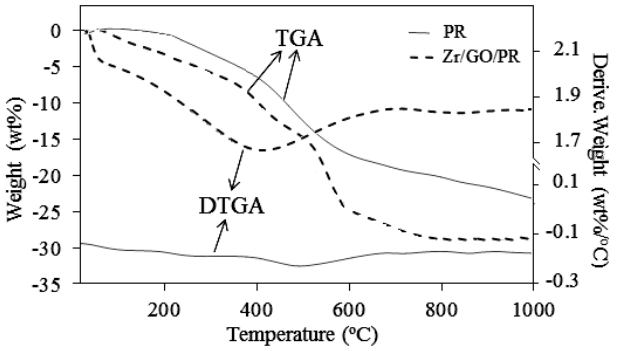

Fig. 2 – (a) TGA and (b) DTG curves of the phenolic samples.

3.3 Ablation properties

The composites are exposed to a high temperature flow in order to evaluate the effects of GO and ZrB_2 on the oxidation behavior of PR. The surface of GO are expected to promote interfacial interactions between GO and resol matrix [13, 14]. The existence of the covalent bonds will increase the density of the filler/polymer interactions, thus improving the filler dispersion into the polymer matrix [15]. The functional groups present in the GO are very useful in making covalent bond linkages with phenolic backbone [16]. It was found that the presence of both graphene oxide sheets and ZrB_2 nanoparticles influences the surface properties [17]. The front side of the samples was directly exposed to the flame at 2000°C for 160 s. When the flame impacted on the sample, heat flux and oxidizing species can be attacked on the sample surface. Meanwhile, B_2O_3 and GO can reflect a large amount of heat to reduce the surface temperature of the sample and weaken oxyacetylene ablation. The boria product of ZrB_2 overflows from the micro-cracks distributed on the surface and decreases the partial pressure of oxidizing species such as CO_2 produced by oxyacetylene torch [18].

The thickness and mass loss measurements were obtained by taking the specimen height and weight difference before and after ablation test. Two samples showed that in terms of the recession rate, the PR composite exhibited higher erosion than Zr/GO/PR nanocomposites. Since the carbon matrix is oxygen sensitive, the PR composite will be largely consumed, which will lead to the high weight loss of the sample [19]. The loading of GO to phenolic resin reduced the mass loss. The ablation rate ratio of 1 wt% GO and 7 wt% ZrB_2 in PR to the neat specimen was a signi-?icantly lower (90%) with insulated surface for transferring heat [18]. The GO sheets were demonstrated to be the key factor for the one-dimensional growth of ZrO_2 (from decomposition of ZrB_2) [20]. The mass loss of Zr/GO/PR composite was about 72% lower than that of PR. The ablative properties of two composites at 2000°C after 160 s are presented in Table 1.

Table 1 – Ablative properties of two composites after 160 s.

Composite	Linear rate (mm/s)	Mass loss (wt%)
PR	0.00970	31.70
Zr/GO/PR	0.00094	8.84

The time-temperature plots of the front side temperatures of the samples were presented in Fig. 3a, and the backside temperatures were measured in situ during exposure in Fig. 3b. When the temperature reached more than 1200°C, B_2O_3 quickly evaporated which can be caused to decrease of temperature from the surface [21]. As illustrated in Fig. 3b, by effectively transferring heat away from the front of the sample, the backside temperatures were greatly reduced. The back face temperature reached 600°C after 160s for PR, but the temperature of Zr/GO/PR composite reached 90°C.

3.4 The microstructure of composites

In order to understand the ablation mechanism, we compared the microstructures of two composites. Figure 4a shows the surface of samples after oxidation. It can be seen that PR has visible structural damage with pitch carbon fibers, but Zr/GO/PR are fully covered by a char layer. Fig. 4b and c shows the FESEM micrographs of the surface of Zr/GO/PR before and after ablation test, respectively. It is found that the carbon fibers were randomly and uniformly dispersed in the matrix without the clumps of fibers in the samples in Fig. 4b. From Fig. 4c for Zr/GO/PR, it is clearly observed that the surface has been covered by the char and ZrO_2 with white color. Electron dispersive spectroscopy (EDS) was performed on the surface of Zr/GO/PR and carbon, oxygen and zirconium are shown in Fig. 4c.

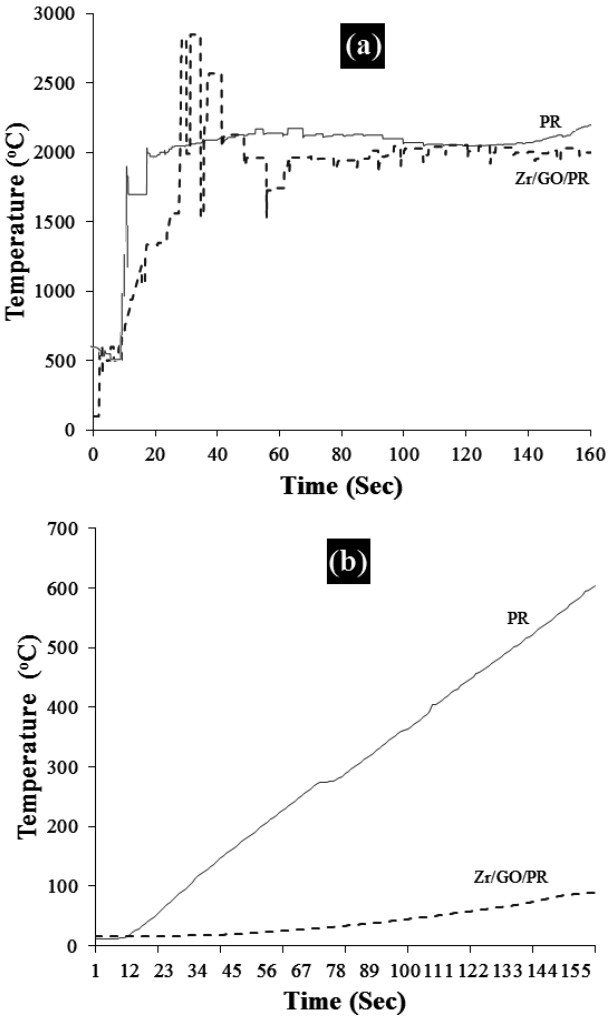

Fig. 3 – The temperatures of (a) surface center and (b) back surface during oxy-acetylene torch test.

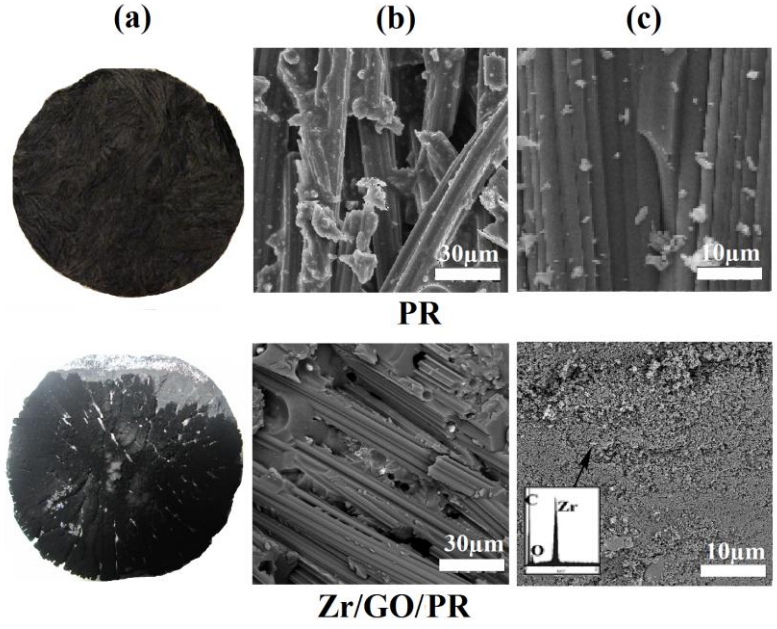

Fig. 4 – FESEM images of the composites: (a) macro-morphologies after oxyacetylene torch test, (b) microstructure of composites before ablation test and (c) the ablated surfaces.

4. CONCLUSIONS

ZrB_2 ceramic nanoparticles, which produced with sol-gel method, combine several desired properties relevant for an application in fiber-reinforced composites. The carbon fiber/resol composite with different inorganic additives (ZrB_2 and GO) were investigated for high temperature (2000°C) operation. A mechanism is proposed to explain possible pathways for conductivity enhancement in the composite. The evaluation of Zr/GO/PR, which had been heated to 2000°C for 160 s, demonstrated that the composite was thermally stable with formation of char compared with PR composite. The linear and mass ablation rates of Zr/GO/PR composites compared with PR decreased by 90% and 72%, respectively.

REFERENCES

1. X. Yang, L. Wei, W. Song, Z. Bi-Feng, C. Zhao-Pui, *Composites: Part B* **45**, 1391 (2013).
2. C. Bao, Y. Guo, B. Yuan, Y. Hu, L. Song, *J. Mater. Chem.* **22**, 23057 (2012).
3. P. Sanoj, B. Kandasubramanian, *J. Comps* **2014**, 15 (2014).
4. 4. L. Liu, H. Li, W. Feng, X. Shi, K. Li, L. Guo, *Corros. Sci.* **74**, 159 (2013).
5. M. Patel, J.J. Reddy, V.V.B. Prasad, J. Subrahmanyam, V. Jayaram, *Mater. Sci. Eng. A* **535**, 189 (2012).
6. E.L. Corral, L.S. Walker, *J. Eur. Ceram. Soc.* **30**, 2357 (2010).
7. G.M. Yadhukulakrishnan, A. Rahman, S. Karumuri, M.M. Stackpoole, A.K. Kalkan, R.P. Singh, S.P. Harimkar, *Mater. Sci. Eng. A* **552**, 125 (2012).
8. F. Tavakoli, M. Salavati-Niasari, *J. Ind. Eng. Chem.* **20**, 3170 (2014).
9. M. Dadkhah, M. Salavati-Niasari, *Mater. Sci. Semicond. Process.* **20**, 41 (2014).
10. M. Ionita, A. M. Pandele, L. Crica, L. Pilan, *Composites: Part B* **59**, 133 (2014).
11. H.A. Becerril, J. Mao, Z. Liu, R. M. Stoltenberg, Z. Bao, Y. Chen, *ACS Nano* **2**, 463 (2008).
12. A.V. Talyzin, T. Szabó, I. Dékány, F. Langenhorst, P.S. Sokolov, V.L. Solozhenko, *J. Phys. Chem. C* **113**, 11279 (2009).
13. F.Y. Yuan, H. B. Zhang, X. Li, H. L. Ma, X. Z. Li, Z. Z. Yu, *Carbon* **68**, 653 (2014).
14. H. Ke, Z. Pang, Y. Xu, X. Chen, J. Fu, Y. Cai, F. Huang, Q. Wei, *J. Therm. Anal. Calorim.* **117**, 109 (2014).
15. Y. Zhan, X. Yang, H. Guo, J. Yang, F. Meng, X. Liu, *J. Mater. Chem.* **22**, 5602 (2012).
16. L.B. Manfredi, O. De la Osa, N. Galego Fernández, A. Vázquez, *Polymer* **40**, 3867 (1999).
17. V. Alzari, V. Sanna, S. Biccai, T. Caruso, Z. Politano, N. Scaramuzza, M. Sechi, R. Sanna, A. Mariani, D. Nuvoli, *Composites: Part B* **60**, 29 (2014).
18. S. Chen, C. Zhang, Y. Zhang, H. Hu, *Composites: Part B* **60**, 222 (2014).
19. J.M. Park, D.J. Kwon, Z.J. Wang, J.U. Roh, W.I. Lee, J.K. Park, K.L. DeVries, *Composites: Part B* **67**, 22 (2014).
20. H. Pang, Q. Lu, F. Gao, *Chem. Commun.* **47**, 11772 (2011).
21. C.L. Zhou, Y.Y. Wang, Z.Q. Cheng, C.H. Wang, J. Fan, C.G. Sun, B.L. Feng, *Adv. Mater. Res.* **105-106**, 199 (2010).